

This is a repository copy of *Mirrored one-nucleon knockout reactions to the  $T_z=\pm 32$   $A=53$  mirror nuclei*.

White Rose Research Online URL for this paper:

<https://eprints.whiterose.ac.uk/id/eprint/103205/>

Version: Published Version

---

**Article:**

Milne, S. A., Bentley, M. A. [orcid.org/0000-0001-8401-3455](https://orcid.org/0000-0001-8401-3455), Simpson, E. C. et al. (22 more authors) (2016) Mirrored one-nucleon knockout reactions to the  $T_z=\pm 32$   $A=53$  mirror nuclei. Physical Review C. 024318. ISSN: 2469-9993

<https://doi.org/10.1103/PhysRevC.93.024318>

---

**Reuse**

Items deposited in White Rose Research Online are protected by copyright, with all rights reserved unless indicated otherwise. They may be downloaded and/or printed for private study, or other acts as permitted by national copyright laws. The publisher or other rights holders may allow further reproduction and re-use of the full text version. This is indicated by the licence information on the White Rose Research Online record for the item.

**Takedown**

If you consider content in White Rose Research Online to be in breach of UK law, please notify us by emailing [eprints@whiterose.ac.uk](mailto:eprints@whiterose.ac.uk) including the URL of the record and the reason for the withdrawal request.

# Mirrored one-nucleon knockout reactions to the $T_z = \pm \frac{3}{2}$ $A = 53$ mirror nuclei

S. A. Milne,<sup>1</sup> M. A. Bentley,<sup>1</sup> E. C. Simpson,<sup>2</sup> P. Dodsworth,<sup>1</sup> T. Baugher,<sup>3,4</sup> D. Bazin,<sup>4</sup> J. S. Berryman,<sup>4</sup> A. M. Bruce,<sup>5</sup> P. J. Davies,<sup>1</sup> C. Aa. Diget,<sup>1</sup> A. Gade,<sup>3,4</sup> T. W. Henry,<sup>1</sup> H. Iwasaki,<sup>3,4</sup> A. Lemasson,<sup>4,6</sup> S. M. Lenzi,<sup>7</sup> S. McDaniel,<sup>3,4</sup> D. R. Napoli,<sup>8</sup> A. J. Nichols,<sup>1</sup> A. Ratkiewicz,<sup>3,4</sup> L. Scruton,<sup>1</sup> S. R. Stroberg,<sup>3,4</sup> J. A. Tostevin,<sup>9</sup> D. Weisshaar,<sup>4</sup> K. Wimmer,<sup>4,10</sup> and R. Winkler<sup>4</sup>

<sup>1</sup>*Department of Physics, University of York, Heslington, York YO10 5DD, United Kingdom*

<sup>2</sup>*Department of Nuclear Physics, Research School of Physics and Engineering, Australian National University, Canberra, Australian Capital Territory 2601, Australia*

<sup>3</sup>*Department of Physics and Astronomy, Michigan State University, East Lansing, Michigan 48824, USA*

<sup>4</sup>*National Superconducting Cyclotron Laboratory, Michigan State University, East Lansing, Michigan 48824, USA*

<sup>5</sup>*School of Computing, Engineering and Mathematics, University of Brighton, Brighton BN2 4GJ, United Kingdom*

<sup>6</sup>*GANIL, CEA/DSM-CNRS/IN2P3, BP55027, F-14076, Caen Cedex 5, France*

<sup>7</sup>*Dipartimento di Fisica dell'Università and INFN, Sezione di Padova, I-35131 Padova, Italy*

<sup>8</sup>*INFN, Laboratori Nazionali di Legnaro, I-35020 Legnaro, Italy*

<sup>9</sup>*Department of Physics, Faculty of Engineering and Physical Sciences, University of Surrey, Guildford GU2 7XH, United Kingdom*

<sup>10</sup>*Department of Physics, The University of Tokyo, 7-3-1 Hongo, Bunkyo-ku, TOKYO 113-0033, Japan*

(Received 13 November 2015; published 24 February 2016)

**Background:** The study of excited states in mirror nuclei allows us to extract information on charge-dependent (i.e., isospin-nonconserving) interactions in nuclei.

**Purpose:** To extend previous studies of mirror nuclei in the  $f_{7/2}$  region, investigating charge symmetry breaking of the strong nuclear force.

**Methods:**  $\gamma$ -ray spectroscopy has been performed for the mirror ( $T_z = \pm \frac{3}{2}$ ) pair  $^{53}\text{Ni}$  and  $^{53}\text{Mn}$ , produced via mirrored one-nucleon knockout reactions.

**Results:** Several new transitions have been identified in  $^{53}\text{Ni}$  from which a new level scheme has been constructed. Cross sections for knockout have been analyzed and compared with reaction model calculations where evidence is found for knockout from high-spin isomeric states. Mirror energy differences between isobaric analog states have been computed, compared to large scale shell-model calculations, and interpreted in terms of isospin-nonconserving effects. In addition, lifetimes for the long-lived  $J^\pi = \frac{5}{2}^+$  analog states in both  $^{53}\text{Mn}$  and  $^{53}\text{Ni}$  have been extracted through lineshape analysis, giving half-lives of  $t_{1/2} = 120(14)$  ps and  $t_{1/2} = 198(12)$  ps, respectively.

**Conclusions:** The inclusion of a set of isovector isospin-nonconserving matrix elements to the shell-model calculations gave the best agreement with the experimental data.

DOI: [10.1103/PhysRevC.93.024318](https://doi.org/10.1103/PhysRevC.93.024318)

## I. INTRODUCTION

In the absence of the electromagnetic interaction, the proton and neutron can be considered as two quantum states of the same particle: the nucleon. In order to distinguish between these particles, they are assigned an isospin quantum number  $t = \frac{1}{2}$  with a projection  $t_z$  along an isospin quantization axis. In this construct the proton is assigned a projection  $t_z = +\frac{1}{2}$  and the neutron  $t_z = -\frac{1}{2}$ , whereby the total isospin projection of the nucleus is given by the sum of the individual isospin projections:  $T_z = (N - Z)/2$  [1]. This concept is also dependent upon the strong nuclear force being charge independent and charge symmetric, and indeed experiment has shown the nucleon-nucleon interactions to be approximately equal for neutron-neutron, proton-proton, and neutron-proton pairs [2]. In the absence of isospin-breaking interactions, one would expect degeneracy between analog states in nuclei of the same mass number [isobaric analog states (IASs)]. Differences in excitation energy of IASs result from isospin-breaking effects such as Coulomb and magnetic effects and any charge dependence of the nucleon-nucleon interaction. The differences between excitation energies of IASs in mirror

nuclei are known as mirror energy differences (MED), which are defined as follows:

$$MED_J = E_{J,T,-T_z}^* - E_{J,T,T_z}^* \quad (1)$$

where  $E_{J,T,T_z}^*$  represents the excitation energy of a state of spin,  $J$ , isospin,  $T$  and isospin projection,  $T_z$ .

Recent work in the  $f_{7/2}$  region, focusing mainly on mirror nuclei, has resulted in the development of a detailed description of MED in terms of these isospin-breaking phenomena—see, for example, Refs. [3–7]. This work has shown the need for the inclusion in the shell-model prescription of an additional isovector term that behaves like a spin-dependent, charge-symmetry-breaking (CSB) term to better reproduce the experimental data [3,4,6,7]. The origin of this phenomenon is still unclear and has usually been accounted for in the model by adding a single repulsive interaction of 100 keV (in addition to the Coulomb interaction) to the two-body matrix elements for  $f_{7/2}$  protons coupled to  $J = 2$  [3,6]. The motivation for this work was to extend previous studies in the region and to study excited states in mirror nuclei at large isospin; in this case the  $T = \frac{3}{2}$  ( $T_z = \pm \frac{3}{2}$ ) pair  $^{53}\text{Ni}$  and  $^{53}\text{Mn}$ .

In this work, we present new data on excited states in the proton-rich  $T_z = -\frac{3}{2}$  system  $^{53}\text{Ni}$  and its mirror  $^{53}\text{Mn}$ . States in  $^{53}\text{Ni}$  have only been tentatively reported in one previous experiment, in which  $^{53}\text{Ni}$  and  $^{53}\text{Mn}$  were populated via  $-3n$  and  $-3p$  removal or fragmentation reactions from a  $^{56}\text{Ni}$  secondary beam at the National Superconducting Cyclotron Laboratory (NSCL) at Michigan State University (MSU) [8]. Due to low statistics, only two transitions could be identified in  $^{53}\text{Ni}$ : at  $\sim 320$  and  $1453$  keV, which are believed to correspond to the  $J^\pi: \frac{5}{2}^- \rightarrow \frac{7}{2}_{\text{g.s.}}^-$  and  $J^\pi: \frac{11}{2}^- \rightarrow \frac{7}{2}_{\text{g.s.}}^-$  transitions, respectively. However, due to its expected long half-life, the excitation energy and half-life of the  $\frac{5}{2}^-$  state could not be accurately measured. The more neutron-rich mirror  $^{53}\text{Mn}$ , however, has a well-known level scheme identified in previous experiments [9–11]. This includes a half-life measurement of the long-lived  $\frac{5}{2}^-$  state, with a measured half-life of  $T_{1/2} = 117(6)$  ps [11].

This work also investigates the use of knockout reactions to populate excited states in exotic proton-rich nuclei and their mirrors in this region [4,8,12]. In terms of direct reactions, mirrored two-nucleon knockout reactions have recently been employed in the study of  $T = 2$  mirror nuclei [8]. In this work, we present a study of a mirror pair using “mirrored” one-nucleon knockout reactions. The direct nature of the population of states in these mirror nuclei, coupled to the isospin symmetric reactions employed, allows significant confidence in the assignment of the states in the exotic  $^{53}\text{Ni}$  nucleus. The present study also allows for a stringent test of the nuclear shell model effective interactions in this region, particularly through MED and cross-section measurements.

## II. EXPERIMENTAL DETAILS

The experiment was performed at the National Superconducting Cyclotron Laboratory (NSCL) at Michigan State University (MSU), where excited states in the mirror nuclei  $^{53}\text{Ni}$  ( $T_z = -\frac{3}{2}$ ) and  $^{53}\text{Mn}$  ( $T_z = +\frac{3}{2}$ ) were populated via one-neutron and one-proton knockout, respectively, from the secondary beams of  $^{54}\text{Ni}$  ( $T_z = -1$ ) and  $^{54}\text{Fe}$  ( $T_z = +1$ )—which are themselves a mirror pair. Due to the symmetry of the reactions used to populate these nuclei (which we refer to as “mirrored knockout”) and therefore their respective excited states, the  $\gamma$ -ray spectra (produced under identical conditions) can be used to identify mirror transitions. This therefore gives high confidence to the spin and parity assignments made by using mirror-symmetry arguments, when the analog states are both particle bound. This new approach to MED studies has already shown great potential in previous work studying proton-rich nuclei in this region [4,8,12].

The secondary beams of interest,  $^{54}\text{Ni}$  and  $^{54}\text{Fe}$ , were produced via the fragmentation of a  $160$  MeV/nucleon  $^{58}\text{Ni}$  primary beam impinging upon a  $802$  mg/cm<sup>2</sup>  $^9\text{Be}$  production target, positioned at the entrance of the A1900 separator. The resulting fragments were separated by the A1900 [13,14], before being transferred to the S800 spectrograph. These secondary beam fragments were then identified from their time of flight (ToF) measured between two plastic scintillators located in the A1900 fragment separator and the object position

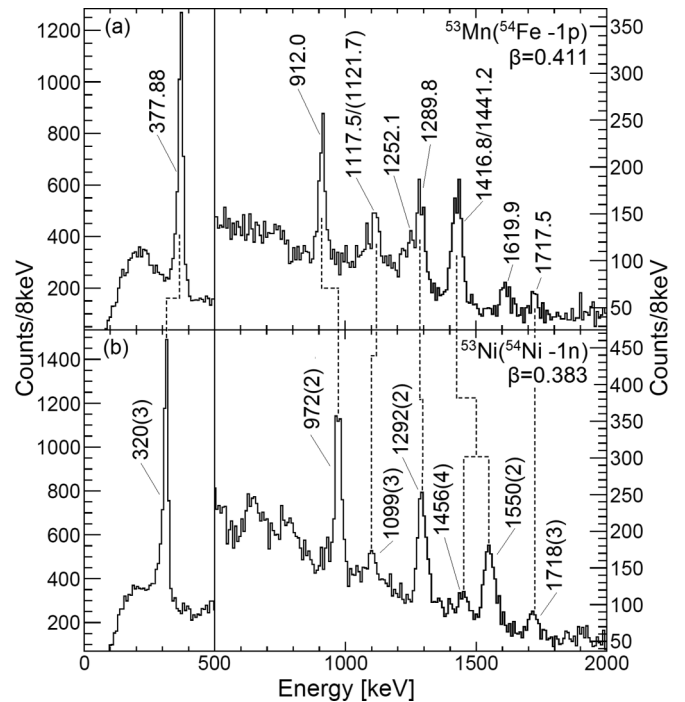


FIG. 1. The Doppler-corrected spectra for  $\gamma$  rays in coincidence with the (a)  $^{53}\text{Mn}$  and (b)  $^{53}\text{Ni}$  fragments, where  $\beta$  was optimized to give the best resolution for the fast transitions. The dashed lines indicate the proposed analog transitions in the mirror nuclei. Transition-energy labels for  $^{53}\text{Mn}$  are shown from previous, more accurate measurements [10].

of the S800 beam line, respectively. At the secondary target position, in the S800 spectrograph [15,16], a  $^9\text{Be}$  reaction target of areal density  $188$  mg/cm<sup>2</sup> was used to populate excited states in the nuclei of interest via mirrored one-nucleon knockout reactions from the  $\sim 87$  MeV/nucleon  $^{54}\text{Ni}$  and  $^{54}\text{Fe}$  secondary beams. In-flight  $\gamma$ -ray decays of the reaction residues were detected by the Segmented Germanium Array (SeGA) detectors [17], positioned in two rings at  $37^\circ$  and  $90^\circ$  with respect to the beam axis. Particle identification was achieved through measuring the energy loss in the S800 ionization chamber and the time of flight through the S800 spectrograph. The  $\gamma$  rays detected by the SeGA detectors were associated with the correct fragments through coincidence conditions.

## III. RESULTS

The Doppler-corrected  $\gamma$ -ray spectra for  $^{53}\text{Mn}$  and  $^{53}\text{Ni}$ , populated via one-nucleon knockout from  $^{54}\text{Fe}$  and  $^{54}\text{Ni}$ , respectively, are presented in Figs. 1(a) and 1(b). A comparison of the spectra demonstrates a clear one-to-one correspondence between the strongest  $\gamma$ -ray peaks observed. However, for some of the weaker transitions, the correspondence is less clear, but some suggestions for this are presented later. Through careful analysis, involving both the use of spectral comparison and, more importantly,  $\gamma$ - $\gamma$ -coincidence analysis, a new level scheme for  $^{53}\text{Ni}$  was deduced, as shown in Fig. 2. The ordering of the transitions has been confirmed by both

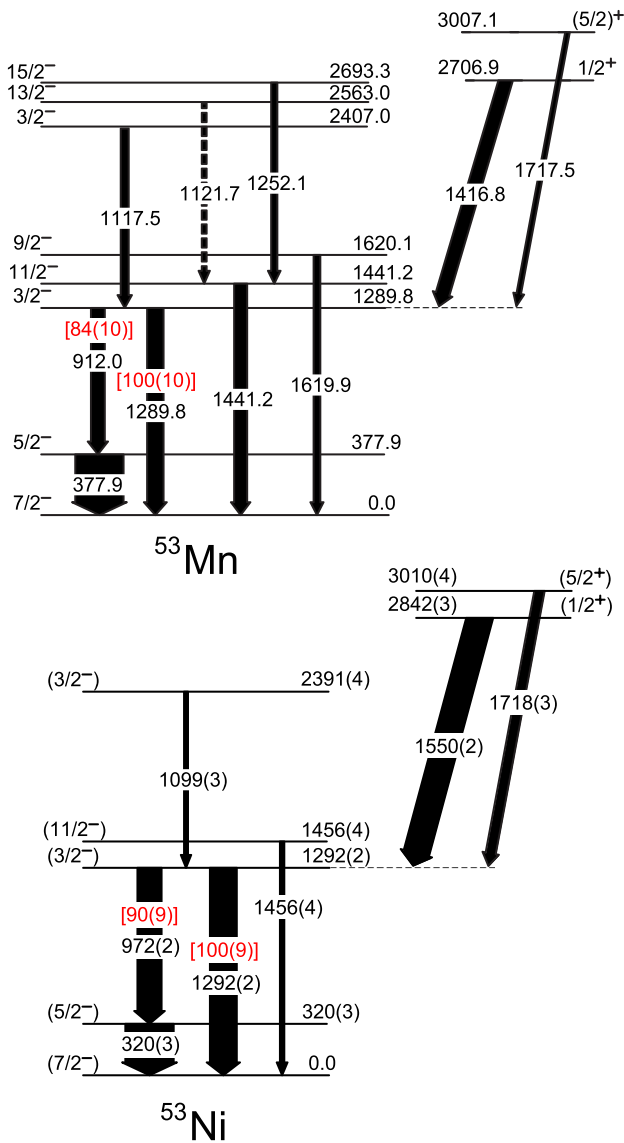


FIG. 2. The energy-level schemes for  $^{53}\text{Ni}$  and  $^{53}\text{Mn}$  as observed in this work. The spins and parities are in parentheses for  $^{53}\text{Ni}$  because the assignments are made on mirror-symmetry arguments. Tentative transitions are indicated by dashed lines. Branching ratios for the  $3/2^-$  level are indicated in red with square brackets and the energy labels used for  $^{53}\text{Mn}$  come from previous, more accurate measurements [10]. The widths of the arrows are proportional to the relative  $\gamma$ -ray intensities observed.

$\gamma$ - $\gamma$ -coincidence analysis and transition intensities. The spins and parities have been assigned based on mirror-symmetry arguments. While the direct, mirrored, reaction process gives confidence in the spin and parity assignments presented, they have not been formally measured and so they are presented here in parentheses. The two transitions previously reported by Brown *et al.* [8], assigned to decays from the yrast  $5/2^-$  and  $11/2^-$  states, are confirmed here. In the previous work [8], the energy of the  $\gamma$  decay from the  $(5/2^-)$  state could not be accurately measured due to its long half-life but has now been

established as 320(3) keV from the energy difference between the 972 and 1292 keV prompt  $\gamma$ -ray transitions.

A detailed understanding of which of the known states in  $^{53}\text{Mn}$  are being populated, and the mechanism through which this occurs, is essential to help establish the new scheme of  $^{53}\text{Ni}$ , populated through the analog knockout process. A partial level scheme of  $^{53}\text{Mn}$ , using information from Ref. [10], is also shown in Fig. 2. Only the transitions observed in this work are shown. One of the states in question, the known  $13/2^-$  state, is only said to be tentatively observed. This is because the transition we observe has a measured energy of 1118(4) keV and is likely to correspond to the 1117.5 keV transition from the  $(3/2^-)$  state, with a possible contribution from the 1121.7 keV transition from the  $13/2^-$  state. It will be shown later that the mechanism that populates the  $15/2^-$  state (which is observed) is also expected to populate the  $13/2^-$  state. Furthermore, the observed transition has a significantly larger relative intensity than the mirror transition in  $^{53}\text{Ni}$  and therefore may be a 1117.5-1121.7 doublet.

Knockout reactions from  $^{54}\text{Ni}$  ( $^{54}\text{Fe}$ ) are expected to populate negative-parity states with  $J^\pi = \frac{7}{2}^-, \frac{3}{2}^-, \frac{5}{2}^-$ , and  $\frac{1}{2}^-$  through removal of  $f_{7/2}^-$ ,  $p_{3/2}^-$ ,  $f_{5/2}^-$ , and  $p_{1/2}^-$  neutrons (protons) near the Fermi level. Being below  $^{56}\text{Ni}$ , the spectroscopic strength to the  $\frac{1}{2}^-$ ,  $\frac{3}{2}^-$ , and  $\frac{5}{2}^-$  states is expected to be weak and, moreover, measured spectroscopic factors for proton removal from  $^{54}\text{Fe}$  to  $^{53}\text{Mn}$  [18] indicate that the bulk of the  $f_{7/2}^-$  spectroscopic strength lies in the  $J^\pi = \frac{7}{2}^-$  ground state. Thus, we expect direct population of all the negative-parity excited states in  $^{53}\text{Ni}$  and  $^{53}\text{Mn}$  to be weak. This is verified in Fig. 2, where it is seen that a significant amount of the intensity observed proceeding through excited states in these mirror nuclei comes from direct population of positive-parity states with  $J^\pi = (\frac{5}{2})^+$  and  $\frac{1}{2}^+$ , through removal of  $d_{5/2}$  and  $s_{1/2}$  neutrons (protons) from  $^{54}\text{Ni}$  ( $^{54}\text{Fe}$ ). In addition to these hole states, there is evidence for higher-spin negative-parity states being populated in both nuclei. For example,  $J^\pi = \frac{11}{2}^-$  states are observed in both nuclei, which cannot be populated by a direct reaction from the ground state of the beam. In addition, higher-spin states are observed more strongly in  $^{53}\text{Mn}$ . These data indicate the presence of isomeric state(s) in the beam(s) and will be discussed later.

The spin assignment of the 3007.1 keV [10] positive-parity state in  $^{53}\text{Mn}$ ,  $J^\pi = (\frac{5}{2})^+$  in Fig. 2, is uncertain. Its first observation in a proton-stripping reaction was shown to correspond to  $l = 2$  [19]. From this, it was assumed to correspond to removal of a  $d_{3/2}$  proton from  $^{54}\text{Fe}$ , and thus the state would have an assignment of  $\frac{3}{2}^+$ . Subsequent papers have since used this assignment. However, the current evaluated nuclear data compilation [10] has this state as a tentative  $\frac{5}{2}^+$ , based on the observed direct decay to the ground state, assumed to be a dipole transition. Earlier work [20] has demonstrated through energy-centroid-shift methods, that this state has a half-life lower limit of 0.84 ps. To gain some further information on this half-life, and to help resolve this assignment, we have performed a Doppler-correction analysis,



whereby the optimum  $\beta$  value to align a  $\gamma$ -ray peak in both the  $37^\circ$  and  $90^\circ$  SeGA rings is determined. This analysis has shown that a  $\beta$  value of  $\sim 0.41$  is required for the other fast transitions in  $^{53}\text{Mn}$  with half-lives  $\sim 1$  ps. These transitions are emitted with the largest value of  $\beta$  because they are emitted from within the target volume. It takes around 8 ps for the beam to traverse the target thickness and therefore, for states with half-lives of the order of 10 ps and greater, the majority of decays take place downstream of the target, where the emitter velocity has been reduced due to energy loss in the target. For example, we find a  $\beta$  value of 0.390 (2) is required to align the  $\gamma$  rays associated with the decay of the long-lived  $J^\pi = \frac{5}{2}^-$  state, which is known to decay downstream of the target. These numbers are consistent with LISE++ [21] calculations that predict a change in  $\beta$  from the center (i.e., the average interaction point) to the back of the target from 0.409 to 0.394. Our analysis for the 1717.5 keV transition yielded a  $\beta$  value of 0.416 (6), where the error comes from our estimate of the uncertainty in aligning the transition energies in the two detector rings. Thus, our experimental data clearly point to the average point of decay being inside the target volume, and so we can put a safe upper limit on the half-life of  $\sim 4$  ps. The 3007.1 keV state is known to decay to the  $\frac{7}{2}^-$  ground state with a 14% branch [22] and, depending on whether it has a spin of  $\frac{3}{2}$  or  $\frac{5}{2}$ , will determine whether it decays via an  $M2$  or  $E1$  transition. Typical transition strengths for  $M2$  transitions in the  $A = 45\text{--}90$  region have been observed in the range of  $0.02 \rightarrow 0.2$  W.u. while  $E1$  transitions have typically been observed in the range of  $(10^{-6} \rightarrow 10^{-4})$  W.u. [23]. With a maximum 4 ps half-life for the 3007.1 keV state, the  $M2$  and  $E1$  transition strengths would be a minimum of 0.3 W.u. and  $6 \times 10^{-7}$  W.u., respectively. This lower-limit  $M2$  transition strength is above the typical range but nevertheless below the recommended upper limit of 1 W.u. proposed in Ref. [23]. Thus, we cannot make a firm assignment here, although the systematics suggest that the current assignment of  $\frac{5}{2}^+$  is more likely. We have assumed this tentative assignment in the following analysis, although the conclusions do not depend strongly on this assumption.

Due to the long half-life [117 (6) ps [11]] of the  $\frac{5}{2}^-$  state in  $^{53}\text{Mn}$  (and presumably in  $^{53}\text{Ni}$ ), decays from this state occur up to a few cm downstream of the target. This has the effect of smearing the effective angle for the SeGA detectors, which in turn yields a broad, asymmetrical lineshape, with a centroid below the correct energy. This presents an opportunity for measurement of lifetimes, through a lineshape analysis, for the analog transitions in this mirror pair. Half-lives were extracted through comparison of experimental  $\gamma$ -ray spectra with simulations generated by using a dedicated lifetime code developed at NSCL [24] utilizing the GEANT4 framework [25]. Although the simulation package also allows for the addition of feeding states, each of which have their own independent lifetimes and intensities, the lifetimes of the observed states feeding the  $\frac{5}{2}^-$  state in  $^{53}\text{Mn}$  are known to be small ( $< 1$  ps) and therefore were not included. It was assumed through mirror-symmetry arguments that these states were also sufficiently short lived to be neglected for  $^{53}\text{Ni}$ . A second-order-polynomial background, which accurately

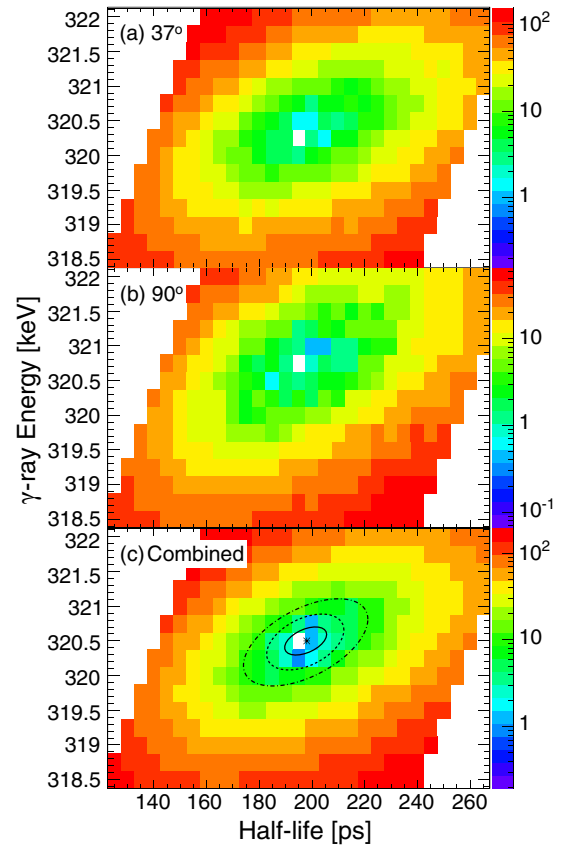


FIG. 3. Plot of  $\chi^2 - \chi_{\min}^2$  for simulated spectra (varying either energy or half-life) fit to the  $^{53}\text{Ni}$  experimental spectra for the  $J^\pi : (\frac{5}{2}^-) \rightarrow (\frac{7}{2}_{\text{g.s.}}^-)$  transition in (a) the  $37^\circ$  SeGA ring and (b) the  $90^\circ$  SeGA ring. (c) The combined  $\chi^2 - \chi_{\min}^2$  plot of panels (a) and (b) where the  $\chi_{\min}^2$  point corresponds to 320.5 keV and 198 ps. Statistical errors in panel (c) are shown by ellipses, whereby the  $\pm 1\sigma$ ,  $\pm 2\sigma$ , and  $\pm 3\sigma$  errors are represented by a solid line, a dashed line, and a dash-dot line respectively. See text for more details.

replicated the experimental backgrounds in either the  $37^\circ$  and  $90^\circ$  SeGA rings, was added to the simulations over the region of lifetime sensitivity. The simulations were produced for both the  $37^\circ$  and  $90^\circ$  SeGA rings and fit to the experimental spectra using a  $\chi^2$  minimization method. For such an analysis, one of the required parameters to produce the simulated lineshape is the  $\gamma$ -ray energy, which in the case of  $^{53}\text{Ni}$  has not yet been accurately determined from the spectrum [the assumed value of 320 (3) keV comes from the subtraction of the 1292 (2) and 972 (2) keV  $\gamma$ -ray energies decaying from the  $\frac{3}{2}^-$  state]. Hence, in this analysis, both the  $\gamma$ -ray energy and half-life were allowed to vary independently. This was done so that both the half-life and energy could be extracted for  $^{53}\text{Ni}$ , and also so that the uncertainty in the  $\gamma$ -ray energy could be accounted for in the result for the extracted half-life.

The resulting  $\chi^2 - \chi_{\min}^2$  plots for  $^{53}\text{Ni}$  are shown in Fig. 3, where Fig. 3(a) shows the results for the simulated fits to the  $37^\circ$  experimental ring and Fig. 3(b) for the  $90^\circ$  ring. It is clear that both the energy and half-life are well determined from this analysis, and also that the results for the two SeGA detector rings are consistent. Hence, it was possible to combine

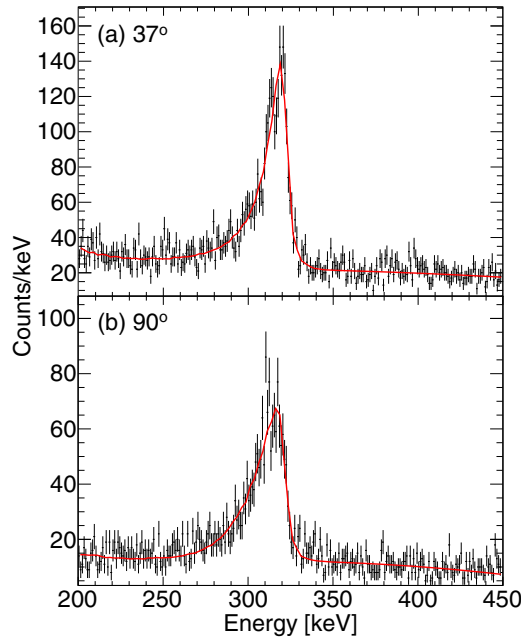


FIG. 4. The best-fit simulated lineshapes (red solid line) to the experimental data (black points), as determined by using a reduced  $\chi^2$ , for (a) the  $37^\circ$  SeGA ring data and (b) the  $90^\circ$  SeGA ring data of the 320 (3) keV  $J^\pi : (\frac{5}{2}^-) \rightarrow (\frac{7}{2}^-)$  transition in  $^{53}\text{Ni}$ .

these results into a single  $\chi^2 - \chi^2_{\min}$  plot, see Fig. 3(c), from which an energy of 320.5 (2) keV and a half-life of 198 (8) ps could be determined. These statistical errors come from the bounds, on each axis, of the  $\pm 1\sigma$  ellipse (solid line), which is derived from  $\chi^2_{\min} + 1$ . To take account of the systematic errors as Ref. [24], in which lifetime measurements were performed for states with a half-life and decay energy very similar to those investigated in this work, and by using an identical simulation code. The systematic error contributions included are as follows: uncertainties due to ambiguities in the geometry of the setup (3%),  $\gamma$ -ray anisotropy effects (1.5%), assumptions in the background (3%), and, finally, effects due to feeding (1%), which in this case would include feeding of the  $\frac{5}{2}^-$  state from short-lived states. (Although the geometrical arrangement of the  $\gamma$ -ray detectors is slightly different in the two experiments, a similar systematic error is assumed.) Adding these uncertainties in quadrature results in an overall systematic error of 4.6%. Taking into account both the systematic and statistical error contributions, a half-life of 198 (12) ps was determined for the  $(\frac{5}{2}^-)$  state in  $^{53}\text{Ni}$ . The lowest  $\chi^2$  fits to both the  $37^\circ$  and  $90^\circ$  SeGA ring data are also shown in Fig. 4. As a check, an identical approach was followed for the  $\frac{5}{2}^-$  state in  $^{53}\text{Mn}$ . However, in this case, the results for the simulated fits to the individual  $37^\circ$  and  $90^\circ$  SeGA rings were only consistent at the  $\sim 2\text{-}\sigma$  level, yielding half-life measurements of 134 (10) and 111 (8) ps, respectively. The discrepancy in these half-life measurements may have resulted due to uncertainties in the target position, which was estimated to be  $\sim 3.5$  mm downstream of the center of the target chamber for this part of the experiment. To account for

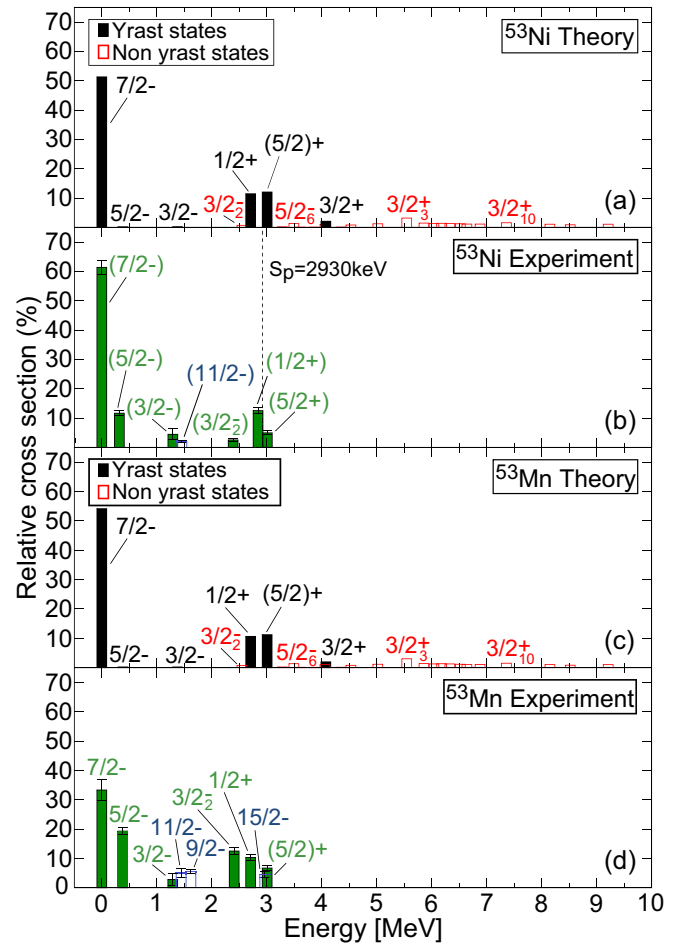


FIG. 5. Calculated and experimental relative cross sections for states in  $^{53}\text{Ni}$  and  $^{53}\text{Mn}$ , populated via one-neutron and one-proton knockout, respectively. The calculations for  $^{53}\text{Ni}$  and  $^{53}\text{Mn}$  [panels (a) and (c)] were obtained by using spectroscopic factors calculated in the shell model, while spectroscopic factors for the positive-parity states were taken from experimental data for  $^{53}\text{Mn}$  and assumed to be the same for  $^{53}\text{Ni}$ . The predicted relative cross sections and energies of both yrast states (black filled) and non-yrast states (red unfilled) are shown. Panels (b) and (d) show the measured relative cross sections to states in  $^{53}\text{Ni}$  and  $^{53}\text{Mn}$ , respectively, where statistical errors are also shown. States colored in green (filled) can be compared with the calculated cross sections, while states colored in blue (unfilled) cannot be populated in direct knockout reactions from the ground state of the projectiles.

this, an additional systematic error of 11 ps (half the difference between the two independent half-life results) was included in the final error analysis for the weighted-average result. This resulted in a weighted-average half-life of 120 (14) ps for the  $\frac{5}{2}^-$  state in  $^{53}\text{Mn}$ , which compares very favorably with the previous measurement of 117 (6) ps [11].

Finally, we have measured, for both nuclei, relative cross sections for knockout to the ground state and all the observed excited states—see Figs. 5(b) and 5(d). These were determined from the measured beam rate by using the efficiency-corrected  $\gamma$ -ray intensities, having subtracted observed feeding from higher-energy states. In this case, further corrections were

made in  $^{53}\text{Mn}$  by accounting for the intensities of previously measured high-energy  $\gamma$  rays (not observed due to low efficiency of high-energy detection) decaying from the  $(\frac{3}{2}^-)$  and  $(\frac{5}{2}^+)$  states with known branching ratios. No such correction was made for  $^{53}\text{Ni}$ , because this would require the uncertain assumption of equal branching ratios between the mirror pair.

#### IV. DISCUSSION

##### A. Knockout cross sections

Calculated and estimated relative cross sections are presented here for the one-neutron knockout from  $^{54}\text{Ni}$  to  $^{53}\text{Ni}$ . The purpose of this analysis is to understand the observed yields, give confidence to the deduced level schemes, and to investigate, more generally, the mirrored-knockout process. The single-nucleon removal cross sections were calculated under the spectator-core approximation by assuming eikonal reaction dynamics [26,27]. The theoretical cross section for populating a specific residue state with spin-parity  $J^\pi$  is given by

$$\sigma_{\text{theor}}(J^\pi) = \sum_{n\ell j} \left( \frac{A}{A-1} \right)^N C^2 S \sigma_{\text{sp}}(n\ell j, S_N + E_x), \quad (2)$$

where  $C^2 S$  is the shell-model spectroscopic factor,  $n\ell j$  denotes the quantum numbers of the nucleon removed, and  $\sigma_{\text{sp}}$  is the single-particle cross section. The mass dependent term is the required center-of-mass correction to the shell-model spectroscopic factors, with  $N = 3$  for the  $fp$  shell [28]. The single-nucleon wave functions were calculated in a Woods–Saxon potential (central plus spin orbit), with diffuseness  $a = 0.6$  fm and spin-orbit strength  $V_{\text{so}} = 6$  MeV. The radius parameters  $r_0$  of the binding potentials were constrained to reproduce the rms radii and binding energies of SkX interaction [29] Skyrme Hartree–Fock calculations. The depth of the central potential was then adjusted to give states at the appropriate effective separation energy  $S_N + E_x$ , where  $S_N$  is the projectile ground-state to residue ground-state nucleon separation energy and  $E_x$  is the residue excitation. Densities from the same Hartree–Fock calculations were used in calculating the core-target  $S$  matrices in the  $tp\bar{p}$  approximation (see, e.g., Ref. [30]). Spectroscopic factors were calculated by using the ANTOINE code [31], using the KB3G [32] interaction in the full  $fp$ -shell space and therefore only the population of negative-parity states is calculated.

The calculated relative cross sections for  $^{53}\text{Ni}$  and  $^{53}\text{Mn}$  residues are shown in Figs. 5(a) and 5(c). To estimate the population of positive-parity states resulting from one-nucleon knockout from the  $sd$  shell, we have used previously extracted spectroscopic factors from transfer reactions onto  $^{53}\text{Mn}$  [18] and assumed that these are the same for  $^{53}\text{Ni}$ . Care needs to be taken with this approach since it is known [27,33] that measured inclusive knockout cross sections are systematically smaller by around a factor of two (for the separation energies concerned here) than cross sections calculated by using theoretical spectroscopic factors from the shell model. Hence, a comparison of cross sections calculated by using a combination of theoretical and experimentally deduced

spectroscopic factors can only be used as a guide. Since the spectroscopic factors used for each member of the mirror pair are identical, the theoretical cross sections in panels (a) and (c) are virtually identical. Including positive-parity states in the calculations in the way described previously, the majority of the intensity ( $\sim 50\%$ ) proceeds directly to the ground state, with  $\sim 20\%$  going to high-lying positive-parity states.

To compare these calculated cross sections with the experimental data, the other processes that may be present need to be considered. The maximum final angular momentum that can result from direct, one-nucleon removal ( $fp$  shell) from  $^{54}\text{Ni}$  or  $^{54}\text{Fe}$ , with a ground state of  $0^+$ , is  $J = \frac{7}{2}$ . However, states of higher spin are observed in the two mirror nuclei. One possibility is that these high-spin states are populated in knockout reactions from high-spin isomeric states in both  $^{54}\text{Fe}$  and  $^{54}\text{Ni}$ . Indeed, a  $10^+$  spin-trap isomer has been previously observed in both  $^{54}\text{Fe}$  and  $^{54}\text{Ni}$ , with measured half-lives of 364 (7) and 152 (4) ns, respectively [34,35]. Both of these isomers are sufficiently long lived to still be present in the secondary beam at the secondary-target position, after their initial population at the production target, since the ToF between these two targets is  $\sim 300$  ns.

One-nucleon knockout from these isomers could, in principle, populate a range of high-spin states from  $\frac{13}{2}^-$  to  $\frac{27}{2}^-$  in the final nuclei and could explain in particular the observation of the  $\frac{15}{2}^-$  and  $\frac{13}{2}^-$  states in  $^{53}\text{Mn}$ . Additional support for this argument comes from cross-section calculations performed (by using the same approach as described above) but assuming direct proton knockout from this isomer in  $^{54}\text{Fe}$  to  $^{53}\text{Mn}$ . Figure 6 shows a theoretically produced decay scheme, using experimental energies and branching ratios, assuming that these states are populated with the theoretically calculated cross sections. These calculations suggest that the entirety of the intensity from the strongly populated states will feed through the  $\frac{15}{2}^-$  and  $\frac{13}{2}^-$  states and collect in the  $\frac{11}{2}^-$  state. This may explain the strong  $\gamma$ -ray transition observed from this state, particularly in  $^{53}\text{Mn}$ . This population of high-spin states does not appear to be mirrored in both daughter nuclei but instead appears to be much stronger in  $^{53}\text{Mn}$ —see Fig. 2. This could be due to different initial isomeric ratios in the secondary beams but will also be due, in part, to the shorter half-life of the  $^{54}\text{Ni}$   $10^+$  isomer compared with that of  $^{54}\text{Fe}$ . This will result in a smaller residual population of the isomer at the secondary target for knockout from  $^{54}\text{Ni}$  to  $^{53}\text{Ni}$ .

The theoretical and measured cross sections for  $^{53}\text{Ni}$  are now compared—see Figs. 5(a) and 5(b). This reveals a fairly good level of agreement, although with a few differences. In particular, the  $(\frac{5}{2})^+$  state appears to have a lower than predicted relative intensity by about a factor of two. However, the  $(\frac{5}{2})^+$  analog state in  $^{53}\text{Mn}$  is known to have two other decay branches, which account for about half the decay strength, but which are not observed here due to their high decay energies. This has already been accounted for in  $^{53}\text{Mn}$  in the  $(\frac{5}{2})^+$  cross-section measurement in Fig. 5(d). If a similar decay pattern exists in  $^{53}\text{Ni}$ , then the measured  $(\frac{5}{2})^+$  cross section in Fig. 5(b) is in reality a factor of two larger and would have a population intensity similar to that of the  $(\frac{1}{2})^+$  state. However, we reiterate that, since the spectroscopic factors for these

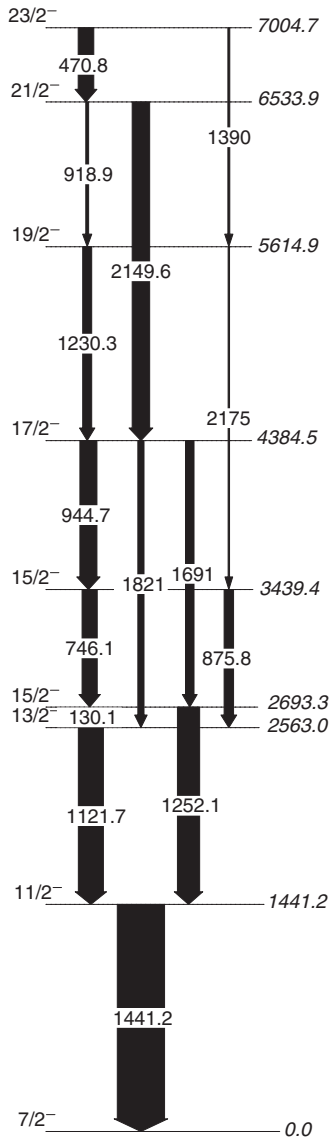


FIG. 6. An energy level scheme of  $^{53}\text{Mn}$  showing the states strongly populated in one-proton knockout from the  $^{54}\text{Fe}$   $10^+$  spin-trap isomer. The population of each state is predicted from cross-section calculations by using the method described in the text, with spectroscopic factors calculated by using the ANTOINE code [31] in the full  $fp$  valence space and with the KB3G interaction [32]. Information on the state energies and branching ratios were used from previous experimental studies on  $^{53}\text{Mn}$  [10].

states were taken from Ref. [18] rather than from shell-model calculations, their branches should only be considered as a guide. Figure 5(b) also shows the population of a number of other low-lying states in  $^{53}\text{Ni}$ , with a much higher relative cross section than expected; see, for example,  $(\frac{5}{2}_1^-)$ ,  $(\frac{3}{2}_1^-)$ , and  $(\frac{3}{2}_2^-)$ . It is probable that these states are populated via fast  $E1$  transitions from a number of low-spin, high-energy, positive-parity states which are expected to be populated [see Fig. 5(a)], with a combined total relative cross section of  $\sim 20\%$ . Indeed, in  $^{53}\text{Mn}$ , several such decay paths are known to exist. This, and decays from other high-lying negative-parity

states, will contribute to the observed low-lying negative-parity strength. In general, and especially having considered these additional decay-branching issues, the agreement between both Figs. 5(a) and 5(b), and between Figs. 5(c) and 5(d), is reasonable.

Finally, we compare the experimental relative-cross-section distributions for the mirror pair—see Figs. 5(b) and 5(d). One would intuitively expect these to be identical, given the mirrored reaction process, but some differences are apparent—e.g., the  $\frac{3}{2}_2^-$  and  $\frac{5}{2}_1^-$  states, and the different relative population of the ground states. First, as has been discussed earlier, there is strong evidence for the presence of the  $10^+$  isomers in the beams—with a much stronger residual population of the isomer at the secondary target for  $^{54}\text{Fe}$ . This accounts for the additional intensity for  $\frac{9}{2}^-$ ,  $\frac{11}{2}^-$ , and  $\frac{15}{2}^-$  in  $^{53}\text{Mn}$ . It has also been pointed out earlier that some higher-lying low-spin states are expected to be populated in both nuclei and could cascade through the low-lying states—such as the  $\frac{3}{2}_2^-$  and  $\frac{5}{2}_1^-$  states. In  $^{53}\text{Ni}$  some of these high-energy states will also be proton unbound ( $S_p = 2930$  keV [36]) and these could decay by proton emission rather than  $\gamma$  decay. In the analysis presented here, the effect would be to artificially increase the ground-state experimental cross section of  $^{53}\text{Ni}$ . This effect also needs to be considered when comparing the experimental and theoretical cross sections for  $^{53}\text{Ni}$ —Figs. 5(a) and 5(c). Finally, the data seems to indicate that the transition observed from the  $\frac{3}{2}_2^-$  state in  $^{53}\text{Mn}$  is a doublet, and that this has artificially inflated the relative cross section to that state of  $^{53}\text{Mn}$  in Fig. 5(d), and hence artificially reduced the apparent cross section to the ground state. In this analysis, it should also be noted that any high-lying states populated that directly feed the ground state will also lead to an overestimate of the relative cross section to the ground state, and such effects may be slightly different between the mirror nuclei.

The conclusion from this analysis is that the relative population of the states in both nuclei can be understood well in terms of the direct knockout processes, assuming symmetry between the spectroscopic factors of the mirror pair and having accounted for the presence of isomeric states in the beams. This again gives confidence in the assignments made for the newly identified states in  $^{53}\text{Ni}$ .

### B. Mirror energy differences

Having established the level scheme for  $^{53}\text{Ni}$ , the experimental MEDs for the  $^{53}\text{Ni}$  -  $^{53}\text{Mn}$  pair can be extracted—these are shown in Fig. 7(a). The work presented here has confirmed the data points at  $\frac{5}{2}^-$  and  $\frac{11}{2}^-$  observed by Brown *et al.* [8] and added the two data points at  $\frac{3}{2}^-$ . In order to interpret these data, large-scale shell-model calculations using the ANTOINE code [31] were performed for the  $^{53}\text{Ni}$  -  $^{53}\text{Mn}$  mirror pair, using the full  $fp$  valence space and the KB3G interaction [32]. No restrictions were placed on the movement of particles between the  $fp$  orbitals. Adopting an identical approach to that described in Ref. [3], four isospin-breaking components, and their subsequent contribution to the MED, were then calculated. These four terms are as follows: (a) The  $V_{\text{CM}}$  term which accounts for the multipole Coulomb interaction



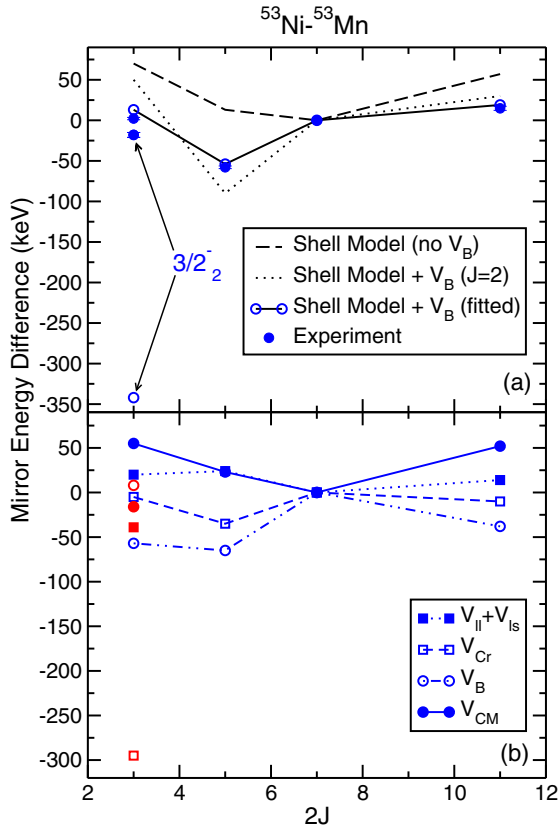


FIG. 7. (a) A comparison between the experimental MED and the shell-model calculations. The dotted line shows the shell-model calculations including the  $V_B$  term for  $J = 2$  only, the solid line shows inclusion of the  $V_B$  parameters extracted from a fit across the shell, and the dashed line shows the calculations with no  $V_B$  term included – see text for details. Data for both  $\frac{3}{2}^-$  states are included, and the lines only connect the yrast states. (b) The four isospin-breaking components of the shell-model calculations (described within the text), the sum of which yields the solid line in (a). For the  $V_B$  term, the parameters extracted from the fit have been used – see text for details. The theoretical data points for yrast states and non-yrast states are colored blue and red, respectively, where the lines only connect the yrast states.

by the addition of Coulomb matrix elements to the effective two-body interaction for protons. (b) The radial term ( $V_{Cr}$ ) is a monopole term which accounts for the Coulomb energy associated with changes in mean nuclear radius, in accordance with Ref. [6]. (c) The  $V_{II}$  and  $V_{Is}$  terms account for Coulomb [6] and electromagnetic spin-orbit shifts [37] of the single-particle levels. (d) The  $V_B$  term represents an additional isovector term for the  $J = 2$  channel, included by adding an additional repulsive term of 100 keV for  $f_{7/2}$  protons at  $J = 2$ . It has been found empirically to be necessary to include this correction term to achieve reasonable agreement with the data [3,6]. Since the monopole terms, generally, have a dependence on  $T_z$ , the effects of  $V_{Cr}$ ,  $V_{II}$ , and  $V_{Is}$  may become enhanced with increasing difference in proton number between the mirror nuclei. This work provides a good test of this shell-model prescription and builds upon previous work [4,8], already

showing excellent agreement at large isospins of  $T_z = \pm 2$  and  $T_z = \pm \frac{3}{2}$ .

The results of the shell-model calculations are shown in Fig. 7(a). As already suggested by Brown *et al.* [8], the inclusion of the isospin-nonconserving ( $V_B$ ) term, shown by the dotted line in Fig. 7(a), results in an improvement in the fit to the experimental data, compared to the dashed line, where no  $V_B$  term has been included. This is consistent with the recent findings in this region—e.g., Refs. [3,4,8]—which have indicated that inclusion of this  $V_B$  term for just  $J = 2$   $f_{7/2}$  matrix elements provides, broadly, a better description of experimental MED. However, rather than using a single isospin-nonconserving matrix element, a recent study [7] has extracted a full set of effective isovector ( $V_{pp} - V_{nn}$ ) matrix elements in the  $f_{7/2}$  shell by fitting the shell model to all experimental MED data so far obtained in the shell. This has yielded matrix elements of  $V_B = -72, +32, +8, -12$  keV for  $J = 0, 2, 4, 6$  couplings of the  $f_{7/2}$  orbital (note again the rise of about 100 keV from  $J = 0$  to  $J = 2$ ). The results of a shell-model calculation, performed when these four matrix elements are added to the two-body interaction for protons, is shown by the solid line in Fig. 7(a). There is an obvious further improvement in the agreement, which is now excellent. It should be noted that the three excited states presented in this work (the  $\frac{3}{2}^-_1$ ,  $\frac{5}{2}^-$ , and  $\frac{11}{2}^-$  states) are included in the fit, which is made up from 93 pairs of excited states in 17 mirror nuclei between  $A = 42$  and 54. Exclusion of these states from the fit changes the result by less than 1 keV. The four components of the shell-model calculation, as described above, are shown in Fig. 7(b), where the values of  $V_B = -72, +32, +8, -12$  keV, extracted from the fit [7], are used.

It is clear from Fig. 7(a) that a significant discrepancy appears for the non-yrast  $\frac{3}{2}^-_2$  state, and an inspection of the various components of the MED in Fig. 7(b) indicates that this is due to the  $V_{Cr}$  term. The  $V_{Cr}$  term is intended [6] to track changes in radii along the yrast band and to determine the resulting MED contribution due to the difference in proton number. In the model, the  $p_{3/2}$  occupancy is tracked to determine the size of the effect [6]. However, the wave function of the  $\frac{3}{2}^-_2$  state contains a significant fraction of a pure  $p_{3/2}$  single-particle configuration, unlike the rest of the states considered. This suggests that this method for calculating the  $V_{Cr}$  term may not be appropriate when pure single-particle excitations of this kind are present.

### C. Half-life of $\frac{5}{2}^-_1$ state

In this work, the half-life of the  $\frac{5}{2}^-_1$  state in  $^{53}\text{Ni}$  [198 (12) ps] was established, allowing a high-precision comparison with its mirror  $^{53}\text{Mn}$  [117 (6) ps [11]]. The  $\gamma$ -ray transition from the state in  $^{53}\text{Mn}$  is known to be highly mixed  $E2/M1$  ( $|\delta| = 0.61$  (8) [38]). It is not possible with the current data to determine a mixing ratio for the transition in  $^{53}\text{Ni}$ , and so no absolute values of the  $B(M1)$  or  $B(E2)$  can be extracted for  $^{53}\text{Ni}$ . However, the data do still constrain the relative values of the  $B(E2)$ s and  $B(M1)$ s as indicated in Figure 8. In the figure, the value of the unknown mixing ratio  $\delta_{Ni}^2$  is allowed to vary freely between 0 and 1, and the experimental data

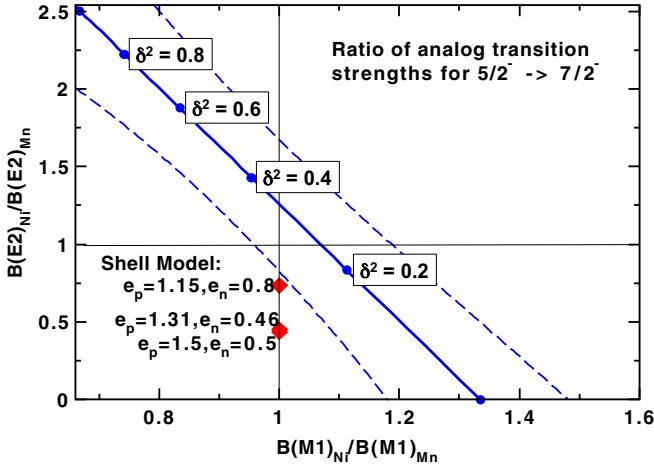


FIG. 8. Data corresponding to the transition between the  $\frac{5}{2}^-$  first-excited state and ground state in both members of the  $A = 53$  mirror pair. The ratio of the analog  $B(E2)$ s is plotted as a function of the ratio of the analog  $B(M1)$ s. The  $E2/M1$  mixing ratio is unknown for the  $^{53}\text{Ni}$  transition, and so the solid line represents the range of data corresponding to values of  $\delta^2$  from 0 to 1. This range of values was chosen because it correspond to the region of the theoretically calculated data points. The dashed lines represent the experimental limits. The red points mark the predictions of the shell-model based on the data in Table I.

for the  $\gamma$ -ray energies, lifetimes, and the known value of  $\delta_{Mn}^2$  are then used to calculate, and plot,  $\frac{B(E2)_{Ni}}{B(E2)_{Mn}}$  vs  $\frac{B(M1)_{Ni}}{B(M1)_{Mn}}$ —see the solid diagonal line. The dashed lines indicate the error bounds resulting from the errors in  $\delta_{Mn}^2$ , the  $\gamma$ -ray energy (in  $^{53}\text{Ni}$ ), and the two half-lives. The region consistent with the experimental data, within error, is therefore between the dashed lines. The range of  $0 \leq \delta_{Ni}^2 \leq 1$  does not contain the full range of possibilities, but was chosen because it is this range that contains the region of similar transition strengths between the mirrors and is the region close to the shell-model predictions. Using the full range of possible  $\delta_{Ni}^2$  values extends the plot to the upper left towards  $(x, y) = (0, \sim 5)$ .

Considering the  $B(E2)$ s initially, if we assume perfect symmetry in the analog wave functions of the states concerned, then intuitively one might expect the  $B(E2)$  in  $^{53}\text{Ni}$  to be reduced compared with its mirror. This is because the number of active valence protons should be very different:  $^{53}\text{Ni}$  will have an (approximately) closed shell of protons, and  $^{53}\text{Mn}$  an (approximately) closed shell of neutrons. The large difference in  $T_z$  in this case should then result in a reduction in  $B(E2)$  for  $^{53}\text{Ni}$  compared with  $^{53}\text{Mn}$ . The data indicates that, if this were the case in reality, then the ratio  $\frac{B(M1)_{Ni}}{B(M1)_{Mn}}$  should be  $\geq 1$ ; i.e.,  $B(M1)$  would be larger for  $^{53}\text{Ni}$ .

The  $B(M1)$  and  $B(E2)$  transition strengths have been calculated in the shell model for both members of the mirror pair, and the results are summarized in Table I. The calculations have been performed using the full set of isospin-breaking terms as described above and use effective  $g$  factors and three different sets of effective charges. The first are the effective charges from du Rietz *et al.*,  $\epsilon_p = 1.15$ ,  $\epsilon_n = 0.8$ ,

TABLE I. Comparison of the experimental and theoretical half-lives,  $B(E2)$ s and  $B(M1)$ s for the analog transitions between the  $\frac{5}{2}^-$  first-excited state and ground state in the  $A = 53$  mirror pair. The  $M1/E2$  mixing ratio is unknown for the  $^{53}\text{Ni}$  transition, and so the individual  $B(E2)$  and  $B(M1)$  are undetermined. Theoretical predictions come from the shell-model predictions using three sets of effective charges, including those of du Rietz *et al.* [39] and Dufour and Zuker [40]. The  $B(M1)$ s are calculated by using effective  $g$  factors ( $g_l^{\text{eff}} = g_l^{\text{free}} \pm 0.1$ , with  $\pm 0.1$  for  $p$ ,  $n$  respectively, and  $g_s^{\text{eff}} = 0.75g_s^{\text{free}}$ ). The shell-model half-lives were calculated by using experimental energies.

	$^{53}\text{Mn}$	$^{53}\text{Ni}$
	Experiment	
$T_{1/2}$ (ps)	117(6) [11]	198(12)
$B(M1)^a$ ( $\mu_N^2$ )	0.0045(4)	
$B(E2)^a$ ( $e^2 \text{ fm}^4$ )	159(34)	
Shell model: $\epsilon_p = 1.15$ , $\epsilon_n = 0.8$ [39]		
$T_{1/2}$ (ps)	232	551
$B(M1)$ ( $\mu_N^2$ )	0.0011	0.0011
$B(E2)$ ( $e^2 \text{ fm}^4$ )	204	150
Shell model: $\epsilon_p = 1.31$ , $\epsilon_n = 0.46$ [40]		
$T_{1/2}$ (ps)	231	678
$B(M1)$ ( $\mu_N^2$ )	0.0011	0.0011
$B(E2)$ ( $e^2 \text{ fm}^4$ )	206.1	92.7
Shell model: $\epsilon_p = 1.5$ , $\epsilon_n = 0.5$		
$T_{1/2}$ (ps)	194	620
$B(M1)$ ( $\mu_N^2$ )	0.0011	0.0011
$B(E2)$ ( $e^2 \text{ fm}^4$ )	267	116

<sup>a</sup>The individual  $B(M1)$  and  $B(E2)$  for  $^{53}\text{Mn}$  have been determined by using the published mixing ratio of  $|\delta| = 0.61(8)$  [38].

derived from mirror nuclei in the upper  $f_{7/2}$  shell [39]; the second are the effective charges from Dufour and Zuker [40]; the third are the “standard” shell-model effective charges of  $\epsilon_p = 1.5$ ,  $\epsilon_n = 0.5$ . Since we are effectively swapping neutron holes for proton holes in this mirror pair, the difference in the  $B(E2)$  should be very sensitive to the effective charges chosen in the shell model—and the table confirms this to be the case.

The shell model overpredicts the half-life of both states significantly in all the calculations, due to the underestimation of the  $B(M1)$  strength—as can be seen from the measured  $B(M1)$  in  $^{53}\text{Mn}$ . In considering the relative values of the  $B(E2)$ s and  $B(M1)$ s between the mirrors, the three sets of shell-model calculations are indicated in Fig. 8. The shell-model, as expected, predicts that the  $B(E2)$  for  $^{53}\text{Ni}$  is indeed significantly lower than for  $^{53}\text{Mn}$ . It is noteworthy that the effective charges from du Rietz *et al.*,  $\epsilon_p = 1.15$ ,  $\epsilon_n = 0.8$ , extracted from the neighboring  $A = 51$ ,  $T_z = \pm \frac{1}{2}$  mirror pair, yield a set of predictions that lie closer to the experimental data. The shell-model underpredicts the  $B(M1)$ s significantly, although they are very weak and hence a detailed comparison with the model is not appropriate. Information on the  $E2/M1$  mixing ratio for  $^{53}\text{Ni}$  is clearly needed in order to make a more complete analysis.

## V. CONCLUSION

In conclusion, new states and  $\gamma$ -ray transitions have been identified in the proton-rich nucleus  $^{53}\text{Ni}$  ( $T_z = -\frac{3}{2}$ ). A new level scheme has been established using arguments based on mirror symmetry (both of the schemes and of the knockout process) and a  $\gamma$ - $\gamma$ -coincidence analysis. The observation of mirrored hole states, based on excitations from  $d_{\frac{5}{2}}$  (though possibly  $d_{\frac{3}{2}}$ ) and  $s_{\frac{1}{2}}$ , is presented. MED have been computed and compared to large-scale shell-model calculations. These are interpreted in terms of isospin-nonconserving effects, demonstrating an improvement in the fit to the data due to the inclusion of a set of isovector isospin-nonconserving matrix elements—in addition to the Coulomb term—which have a strong  $J$  dependence. Detailed comparisons have been made between experimental and theoretical relative cross sections

for one-nucleon knockout reactions leading to the mirror pair. A high degree of symmetry is observed in the knockout process, with differences discussed in terms of binding-energy effects and the presence of isomers in the secondary beams. A reasonable agreement with the theoretical cross sections is obtained. Finally, a comparison of mirrored lifetimes has been made possible by measurement of the long-lived  $\frac{5}{2}^-$  yrast state in  $^{53}\text{Ni}$  by using lineshape analysis, resulting in a half-life measurement of 198 (12) ps.

## ACKNOWLEDGMENTS

This work was supported by the UK Science and Technology Facilities Council under Grants No. ST/J000124, No. J000051, and No. J000132, and the National Science Foundation (NSF) under Grant No. PHY-1102511.

- 
- [1] E. Wigner, *Phys. Rev.* **51**, 106 (1937).
  - [2] R. Machleidt and I. Slaus, *J. Phys. G* **27**, R69 (2001).
  - [3] M. A. Bentley and S. M. Lenzi, *Prog. Part. Nucl. Phys.* **59**, 497 (2007).
  - [4] P. J. Davies *et al.*, *Phys. Rev. Lett.* **111**, 072501 (2013).
  - [5] J. Ekman, C. Fahlander, and D. Rudolph, *Mod. Phys. Lett. A* **A20**, 2977 (2005).
  - [6] A. P. Zuker, S. M. Lenzi, G. Martínez-Pinedo, and A. Poves, *Phys. Rev. Lett.* **89**, 142502 (2002).
  - [7] M. A. Bentley, S. M. Lenzi, S. A. Simpson and C. Aa. Diget, *Phys. Rev. C* **92**, 024310 (2015).
  - [8] J. R. Brown *et al.*, *Phys. Rev. C* **80**, 011306 (2009).
  - [9] P. Fintz *et al.*, *J. Phys. (Paris)* **40**, 511 (1979).
  - [10] H. Junde, *Nucl. Data Sheets* **110**, 2689 (2009).
  - [11] S. Gorodetzky *et al.*, *Nucl. Phys.* **85**, 519 (1966).
  - [12] M. A. Bentley *et al.*, *Mod. Phys. Lett. A* **25**, 1891 (2010).
  - [13] D. J. Morrissey, B. M. Sherrill, M. Steiner, A. Stolz, and I. Wiedenhoever, *Nucl. Instrum. Methods Phys. Res., Sect. B* **204**, 90 (2003).
  - [14] D. J. Morrissey, *Nucl. Instrum. Methods Phys. Res., Sect. B* **126**, 316 (1997).
  - [15] D. Bazin, J. A. Caggiano, B. M. Sherrill, J. Yurkon, and A. Zeller, *Nucl. Instrum. Methods Phys. Res., Sect. B* **204**, 629 (2003).
  - [16] J. Yurkon, D. Bazin, W. Benenson, D. J. Morrissey, B. M. Sherrill, D. Swan, and R. Swanson, *Nucl. Instrum. Methods Phys. Res., Sect. A* **422**, 291 (1999).
  - [17] W. F. Mueller, J. A. Church, T. Glasmacher, D. Gutknecht, G. Hackman, P. G. Hansen, Z. Hu, K. L. Miller, and P. Quirin, *Nucl. Instrum. Methods Phys. Res., Sect. A* **466**, 492 (2001).
  - [18] N. G. Puttaswamy *et al.*, *Nucl. Phys. A* **401**, 269 (1983).
  - [19] E. Newman and J. C. Hiebert, *Nucl. Phys. A* **110**, 366 (1968).
  - [20] P. D. Georgopoulos, E. J. Hoffman, and D. M. Van Patter, *Nucl. Phys. A* **226**, 1 (1974).
  - [21] O. B. Tarasov and D. Bazin, *Nucl. Nucl. Instrum. Methods Phys. Res., Sect. B* **266**, 19 (2008).
  - [22] R. L. Schulte, J. D. King, and H. W. Taylor, *Nucl. Phys. A* **243**, 202 (1975).
  - [23] P. M. Endt, *At. Data Nucl. Data Tables* **23**, 6 (1979).
  - [24] A. Lemasson *et al.*, *Phys. Rev. C* **85**, 041303 (2012).
  - [25] S. Agostinelli *et al.*, *Nucl. Instrum. Methods Phys. Res., Sect. A* **506**, 250 (2003).
  - [26] P. G. Hansen and J. A. Tostevin, *Annu. Rev. Nucl. Part. Sci.* **53**, 219 (2003).
  - [27] A. Gade *et al.*, *Phys. Rev. C* **77**, 044306 (2008).
  - [28] A. E. L. Dieperink and T. de Forest, *Phys. Rev. C* **10**, 543 (1974).
  - [29] B. A. Brown, *Phys. Rev. C* **58**, 220 (1998).
  - [30] J. S. Al-Khalili and J. A. Tostevin, *Phys. Rev. Lett.* **76**, 3903 (1996).
  - [31] E. Caurier and F. Nowacki, *Acta Phys. Pol., B* **30**, 705 (1999).
  - [32] A. Poves, J. Sanchez-Solano, E. Caurier, and F. Nowacki, *Nucl. Phys. A* **694**, 157 (2001).
  - [33] J. A. Tostevin and A. Gade, *Phys. Rev. C* **90**, 057602 (2014).
  - [34] E. Dafni *et al.*, *Phys. Lett. B* **76**, 51 (1978).
  - [35] D. Rudolph *et al.*, *Phys. Rev. C* **78**, 021301 (2008).
  - [36] M. Wang, G. Audi, A. H. Wapstra, F. G. Kondev, M. MacCormick, X. Xu, and B. Pfeiffer, *Chin. Phys. C* **36**, 1603 (2012).
  - [37] J. A. Nolen and J. P. Schiffer, *Annu. Rev. Nucl. Sci.* **19**, 471 (1969).
  - [38] P. H. Vuister, *Nucl. Phys. A* **91**, 521 (1967).
  - [39] R. du Rietz *et al.*, *Phys. Rev. Lett.* **93**, 222501 (2004).
  - [40] M. Dufour and A. P. Zuker, *Phys. Rev. C* **54**, 1641 (1996).